REVIEW OF SCIENTIFIC INSTRUMENTS

Isothermal furnace for long-term in-situ and real-time X-radiography solidification experiments

M. Wegener,[1, a)] C. Dreissigacker,[1] M. Becker,[1] and F.Kargl[1, 2, b)]
[1)]*Institut für Materialphysik im Weltraum, Deutsches Zentrum für Luft- und Raumfahrt (DLR), 51170 Köln, Germany*
[2)]*Foundry Institute, RWTH Aachen University, Intzestraße 5, 52072 Aachen, Germany*

(Dated: 4 March 2021)

A new X-ray isothermal furnace has been developed, suitable for in-situ observations of semi–solid processes including the transition from dendritic to globulitic grain morphology and grain coarsening in metallic samples. A homogeneous, isothermal temperature field is achieved using a novel heater concept. The furnace structure is sandwich-like with heating elements positioned in the beam line and parallel to the sample. Planar heat transfer to the sample enables measurements with low cooling rates and a minimized temperature gradient. Cooling rates from 0.1 K min^{-1} to 15 K min^{-1} can be controlled in the temperature range 1170 K-670 K. The furnace setup is integrable in the existing rotatable laboratory X-ray facility (X-RISE) at the German Aerospace Center (DLR).In this setup, an effective pixel size of 3 um and a field of view of 8 mm in diameter can be achieved. Preliminary solidification and semi-solid experiments in the hypoeutectic alloy systems Al-Ge and Al-Cu, inoculated with Al-5Ti-1B grain refiner, are presented. They indicate a very uniform temperature distribution in the sample.

I. INTRODUCTION

To study microstructure formation of metallic alloys, in-situ X-ray observations are often carried out as they benefit from the attenuation contrast of the different alloying elements and give insights into dynamic phenomena during solidification[1–3]. Pioneering work of in-situ observation of metal alloy melts began with the use of laboratory X-ray sources to investigate, for example, solute redistribution during solidification and boundary layer propagation by Stephenson and Beech[4] in 1977 and particle-interface interactions by Kaukler and Rosenberger[5] in 1994. Spatial and temporal resolution for X-ray radiography improved later, when experiments were performed at high brilliant synchrotron sources[1] or using advanced X-ray tube and detector technologies[6].Laboratory-based X-ray sources have become a powerful tool in the last years with obvious flexibility benefits over synchrotron sources[7–9]. Advances in image technology, detector development and high-resolution X-ray sources combined with a wide range of furnace setups enabled the investigation of microstructure during solidification in institute laboratories and on microgravity platforms; sounding rockets or parabolic flights, for example[10–13]. Columnar and equiaxed dendritic growth[9,14–17], grain coarsening[18,19] and grain fragmentation[20,21] effects have been studied using thin samples with in-situ X-ray techniques under both terrestrial and microgravity conditions. To observe long term coarsening processes and the transition from globulitic to dendritic growth morphology, a gradient-free temperature field in the sample over a long period of time is required. Preliminary experiments with the near–isothermal furnace (ITF) developed by Becker et al.[7] showed a small temperate gradient from the center of the sample. This gradient was previously reported by Becker et al.[7] to be cooling rate dependent. For a low cooling rate of 1 K min^{-1} a gradient of 0.1 K mm^{-1} was reported. The gradient is caused by the radial heat input from the heater around the Boron Nitride cylinder. Figure 1 shows a hypo-eutectic Al-Ge sample inoculated with 5wt. % Al-5Ti-1B grain refiner and processed in the ITF. The sample is first solidified with 10 K min^{-1} then cooled further at 0.1 K min^{-1} for an hour. The secondary cooling rate is a factor of 10 lower than the one used for the gradient calculated by Becker et al.[7]. Hence, a smaller temperature gradient is expected. Nonetheless, it is not neglectable. For samples with smaller diameter than the one reported by Becker et al.[7] the growing grains appear to develop an irregular shape and to agglomerate while the outer zone is re-melted, as shown in Figure 1. For samples with the typically used larger diameter the Aluminum dendrites are re-melted with solid Al accumulating in the center of the sample (not shown). Here several phenomena, caused by the temperature gradient, seems to influence the developing microstructure. For larger cooling rates, the melt undercools and promotes heterogeneous nucleation[22]. Al-dendrites nucleate and grow. At smaller cooling rates, due to a higher melt temperature next to the heaters, the melt here slightly overheats above the liquidus temperature. This can cause remelting of the Al-dendrites or promotion of Temperature Gradient Zone Melting (TGZM)[3,23], while in the inner zone of the sample isothermal coarsening of the solid aluminium can be observed. To avoid those effects and therefore to enable stable long-term semi-solid processing experiments a new isothermal furnace (ITF2) was developed with a reduced thermal gradient inside the sample. State of the art furnaces heat either circular samples radially or rectangular samples in a so-called coupled Bridgman-type furnace with an adiabatic zone between both heaters. Both types of setups result in a small gradient towards the center of the sample[7,9]. This leads to zone melting towards the outer rim during long-term coarsening experiments. To overcome this limitation, the concept of a planar heat input horizontal to the sample

[a)]Present address: Institut für Werkstoffwissenschaften und -technologien, Fachgebiet Struktur und Eigenschaften von Materialien, Technische Universität Berlin, 10623 Berlin, Germany
[b)]Electronic mail: florian.kargl@dlr.de

instead of a radial heat input was used. A similar concept was presented within the XRMON-SOL furnace[8], in which eight independently controlled heaters are positioned around a circular sample. Since the individual adjustment of the eight zones to achieve isothermal conditions is a challenging task, our concept with two zones above and below the sample is easier to control. It must be noted that in XRMON-SOL the eight heaters are still positioned around the circular sample to keep the X-ray transmitting part free of the metal wire used for resistance heating, which would impede the image analysis. Hence, also in this setup an adiabatic zone is setup which relies on heat transport in the sample surrounding structure as well as their sufficient insulation. ITF2 uses thin Graphite foil heaters, which are X-ray transparent. With this arrangement heat input is homogeneous across the entire sample with no interaction of the X-ray images. Another requirement for the new design was an improved and more precise temperature measurement of the sample. Other X-ray transparent furnaces developed so far do not allow for a direct measurement of sample temperature. The reason is that measuring the temperature with a thermocouple inside the melt can act as a heat sink and trigger nucleation. A contactless temperature measurement, like pyrometry-based measurement technique, is difficult due to the setup geometry and insulation material. Furthermore, an accurate pyrometry-based measurement would require a well-defined surface, which is not possible on a nucleating melt. In ITF2, three thermocouples measure the melt temperature next to the sample, while two other thermocouples monitor the heater temperature. In addition, a supplementary thermocouple (here TC_{Sample}) can be placed directly in the melt, but was only used to prove the homogeneous temperature distribution in the center of the furnace. The new furnace can be mounted in DLR's X-RISE facility[24]. Besides the detailed furnace design, we also report on long-term semi-solid experiments with controlled cooling rates. A sample setup aligned horizontally with respect to gravity suppresses convection in the melt. In-situ observation of the re-melting and coarsening of grains enables the study of semi-solid processes and the globular growth of grains at small cooling rates between $0.1\,\mathrm{K\,min^{-1}}$ and $15\,\mathrm{K\,min^{-1}}$.

II. FURNACE DESIGN

For the new furnace design a compact sandwich-like construction is chosen. This allows the sample to be heated from above and below assuring homogeneous and uniform heat input into the sample. A furnace diameter of 60 mm is selected to compensate for heat loss at the borders and encourage a homogeneous temperature zone in the center. Figure 2 demonstrates the arrangement of the furnace. The furnace consists mainly of Boron Nitride plates, enclosed by Graphite foam from Schunk Carbon Technology and Rescore® 920 (Al2O3/SiO2) as insulation. Each material is selected to assure optimal X-ray transmission and a constant coefficient of thermal expansion in a temperature range between 330 K and 1200 K. The insulation is designed to prevent heat loss and is robust enough to protect the furnace

1.jpg

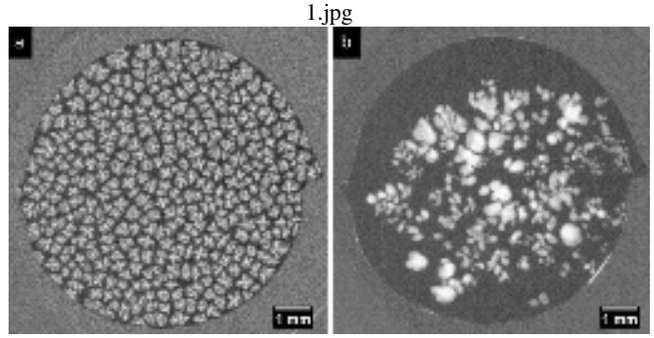

FIG. 1. Microstructure evolution of an Al-33wt.%Ge, inoculated with 5wt.% Al-5Ti-1B sample, processed in the near-isothermal furnace developed at the DLR [4]. a) The sample is solidified with $10\,\mathrm{K\,min^{-1}}$. The process is stopped, 10 s after the first dendrite appeared in the FOV. Al-dendrites grow homogeneously distributed in the whole melt. b) The same sample after one hour, further cooled down with $0.1\,\mathrm{K\,min^{-1}}$. A small temperature gradient caused agglomeration of the Al-dendrites in the center of the sample, while the outer zone is re-melted. Reprinted with permission from M.Wegener, Morphological transitions in Al-Ge alloys observed with in-situ X-radiography, Ph.D. dissertation (RWTH Aachen University, 2021[25]).

core against movement and rotation, especially during mounting inside the X-RISE facility or during parabolic flights. Two meander-shaped, identical Graphite foil heaters are made from SIGRAFLEX®, foil F01513TH from SLG Carbon. The heaters with a thickness of 150 µm are placed between the Boron Nitride plates equidistant from the sample. Additional thin Graphite foils (SIGRAFLEX®, F01513TH, 150 µm) are placed between the Boron Nitride plates to ensure efficient and fast thermal homogenization. The Graphite foil shows anisotropic heat conductivity with a faster heat transfer par-

2.jpg

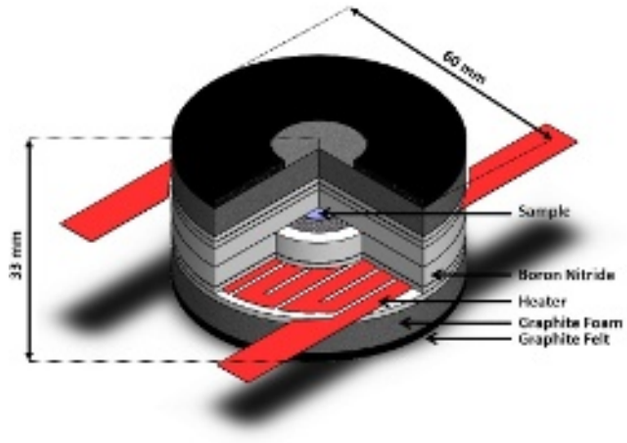

FIG. 2. Schematic of the furnace ITF2. The sample is placed centrically in a pocket between Boron Nitride plates (15 mm in total). Two thin Graphite heaters (150 µm, highlighted in red) heat the furnace from above and below. Graphite foam (7 mm each) and felt (2 mm each) isolate the setup against the environment.

allel to its surface and an order of magnitude lower heat transport through its thickness. To protect the Graphite foil from reaction with oxygen, the setup is operated under vacuum. The heaters can reach a temperature of 1200 K within 300 seconds of continuous heating with 200 W. This results in a sample temperature of 1170 K, measured in the melt, at 65 W holding power. For long-term experiments with several solidification cycles a moderate sample temperature between 823 K-923 K is suggested. Above 670 K maximum cooling rates of 15 K min^{-1} are possible. Limited by the accuracy and controllability of the thermocouples, the furnace can be cooled at a minimum rate of 0.1 K min^{-1}. A second requirement for the new design was an improved and more precise temperature measurement of the melt. In order to achieve this, five type-K thermocouples with a diameter of 0.5 mm are incorporated to monitor the furnace temperature. Three thermocouples sit close to the sample (TC1-TC3) and two near the heaters (TC4-TC5). The thermocouples are arranged radially around the sample, displayed in Figure 3. The thermocouples (TC1-TC3) are inserted in the lower Boron Nitride Plate with which they perfectly line up. Additionally they were fixed with heat resistant ceramic clue, to fix their position permanently and improve the heat transfer. For a quantitative estimation of the heat distribution within the furnace and to calculate the heat loss towards the borders, the thermocouples have different radial distances from the sample. A fourth type-K thermocouple with a diameter of 0.25 mm (here TC$_{Sample}$) can be used to monitor the temperature inside the sample or in the cartridge surrounding, e.g. at the bottom plate. The maximum sample size is 500 µm deep and 18 mm in diameter to suit a milled pocket. However, most experiments were performed on samples with a thickness of 200 µm. Samples with a diameter of 8 mm showed the most homogeneous temperature field inside the sample. To ensure fast temperature homogenization, the sample is encapsulated between two Graphite foils (150 µm). Those foils reduce the depth of the pocket and also prevent a reaction between the Boron Nitride plates of the furnace and the liquid melt. A slight compression of the sample is achieved by compression of the whole furnace. Four screws bolt an Aluminum plate on top of the furnace setup to a bottom plate. Adjusting the length of the screws adapts the pressure on the sample. Two pieces of Graphite felt between the Rescore® 920 and outer layer of Boron Nitride minimize the pressure on the furnace parts. The pressure on the sample leads to a more uniform sample thickness. Sample thickness and diameter are important variables influencing the X-ray transmission and possible radiographic contrast. Thinner samples reduce convection in the melt, but limit the free growth of the dendrites in the third dimension perpendicular to the plane of the sample[26].

III. X-RAY EXPERIMENTAL SETUP

The furnace is installed in a multifunctional experiment cartridge, developed at the Institute of Material Physics in Space, DLR[7] (cf. Figure 4). The cartridge provides connections for power, thermocouples, active water cooling and is sufficiently gas tight to enable evacuation. The cartridge is installed in the X-ray facility described in detail by Klein et al.[24]. The X-ray facility is 90° rotatable, enabling measurements with gravity acting parallel or perpendicular to the sample surface. A thin Tungsten film on an Aluminum target is used as a X-ray source, generating a spot size of 3 µm with a

3.jpg

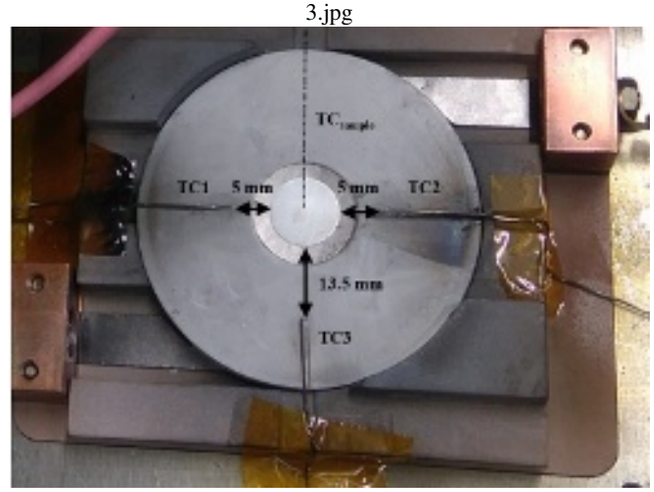

FIG. 3. Photography of the thermocouples installed inside the furnace. TC$_{Sample}$ enables direct measurement of the temperature inside the melt, while TC1-TC3 monitor the temperature near the sample. Reprinted with permission from M.Wegener, Morphological transitions in Al-Ge alloys observed with in-situ X-radiography, Ph.D. dissertation (RWTH Aachen University, 2021[25]).

4.jpg

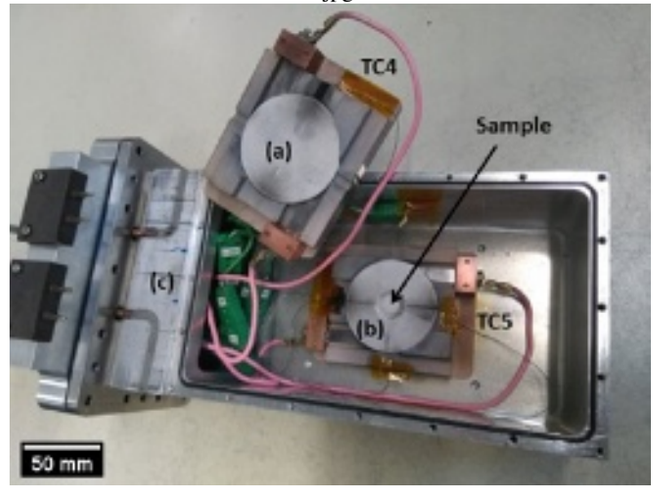

FIG. 4. Photograph of the experimental cartridge containing the isothermal furnace. a) Upper part of the furnace, which can be lifted for sample changing. b) Bottom part of the furnace, symmetric to the upper part and directly connected to the water-cooled bottom plate of the cartridge c) Vacuum-sealed and water-cooled cartridge. Reprinted with permission from M.Wegener, Morphological transitions in Al-Ge alloys observed with in-situ X-radiography, Ph.D. dissertation (RWTH Aachen University, 2021[25]).

X-ray power of <4 W. The operating voltage and current used for the measurements were 50 kV and 80 µA. The distance between X-ray source and sample is 44 mm. The distance between the detector and the X-ray source is 150 mm. This results in a geometrical magnification, M, of approximately 3.4 and a field of view (FOV) of 8 mm in diameter (Figure 5). The detector system is composed of a digital camera (Vosskühler 11000) with a 24 x 36 mm CCD sensor and a structured CsI scintillator. The CCD sensor has 4024 x 2680 pixels with a native pixel size of 9 µm and a pixel depth of 12 bits. This leads to a calculated effective pixel size of approximately 3 µm. The camera is actively cooled to reduce electronic noise. To improve the X-ray permeability of the cartridge, the Aluminum windows in the bottom and top plate where the beam passes through were replaced by windows of 400 µm self–adhesive Kapton-foil. In total, 15 mm of Boron Nitride, 4 mm of Graphite foam 0.9 mm of Graphite foil and 2 mm Rescore® 920 are in the beam path, in addition to the sample.

IV. PERFORMANCE TEST AND PRELIMINARY RESULTS

Preliminary experiments have been carried out using the hypo-eutectic alloys Al-20 wt.%Ge inoculated with 1 wt. %Al-5Ti-1B and Al-20 wt.%Cu inoculated with 0.01 wt.% Al-5Ti-1B grain refiner. Both systems Al-Cu and Al-Ge provide excellent X-ray contrast due to the large difference in atomic weights of Ge (72.63 u), Cu (63.55 u) and Al (26.98 u). Working with compositions in the hypo-eutectic regime Al-dendrites (light grey) will grow in a Cu/Ge-enriched melt (dark grey) during solidification. The samples were made from 6N pure Aluminum provided by Hydro Norsk and 4N pure Germanium from Leibniz–Institut

5.jpg

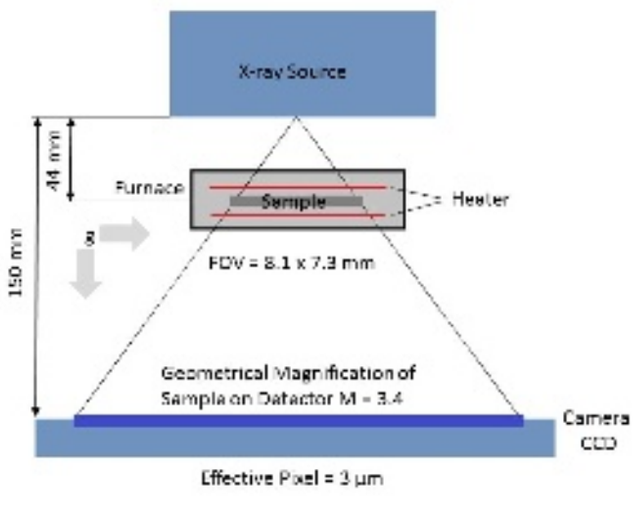

FIG. 5. Sketch of the X-ray imaging system. The distance between the X-ray source, the camera and the sample in the furnace is displayed.

für Kristallzucht (IKZ), Berlin and 4N pure Copper from Alfa Aesar. The added grain refiner is a master alloy from AFFILIPS master alloy (KBM), Netherlands, and has industrial standard. 15 mm long rods with diameters of 8 mm for the Al-20 wt.%Ge and 12 mm for the Al-20 wt.%Cu alloys were cast using a steel mold and a cold crucible furnace, respectively. Each rod was sectioned into approximately 1 mm thick sample discs which were subsequently polished down to 200±10 µm thickness before being installed into the ITF2. All experiments were run under $1\text{x}10^{-4}$ mbar vacuum or better. Solidification was triggered by powering-down the furnace with a constant cooling rate. All samples were aligned horizontally to minimize convection. Consecutive furnace characterization experiments were carried out by subjecting the Al-20 wt.%Cu sample to several heating and cooling cycles with different cooling rates. Figure 6 a)-c) show temperature-time-curves for cooling rates of $1\,\text{K}\,\text{min}^{-1}$, $2\,\text{K}\,\text{min}^{-1}$, and $5\,\text{K}\,\text{min}^{-1}$, respectively. An exact determination of the liquidus temperature is not possible with this setup. To give an idea of the possible range of liquidus temperature an uncertainty of ± 1 wt.% of the alloy composition was assumed and the impact on liquidus temperature[27] is displayed in Figure 6 a). The insets in each figure focus on the eutectic transformation. It can be observed that the temperatures TC1-TC3 precisely follow the set cooling rate after some initial transient period. As expected, TC3 shows the lowest temperature as it is positioned farthest from the furnace center (19.5 mm). TC1 and TC2 are positioned only about 11 mm from the furnace center and show a higher temperature. Differences between TC1 and TC2 can be ascribed to small deviations between the thermocouple position and contact to the surrounding surfaces. The effect is cooling rate dependent but still within the expected error of about 1 to 2 K for the cooling rates analyzed. It was also observed that the differences in temperature between the thermocouples TC1/TC2 and TC3 increase with increasing cooling rate. The increase is about 2 K when increasing the cooling rate from $1\,\text{K}\,\text{min}^{-1}$ to $5\,\text{K}\,\text{min}^{-1}$. TC_{Sample} shows a temperature which is about 1 K higher than the temperature measured by TC2. The highest deviation in temperature is measured between the temperature in the melt TC_{Sample} and TC3, which is reasonable as they are the furthest apart. During commissioning the thermocouple placed within the sample, TC_{Sample}, was used to monitor the liquidus temperature of the melt T_L and the temperature of the eutectic phase transition T_E. The diameter of the thermocouple was chosen to be in the size of the thickness of the sample, to ensure full wetting, when the sample is liquid. The eutectic concentration and temperature of the phase transition is well known for the systems and was used to validate the exact temperature of the melt inside the furnace. To make transitions more visible Figures 6 d) and e) show temperature difference curves as a function of time. A fitted baseline with constant slope was subtracted from the measured curves. The baseline was fit to the intermediate range times well away from the liquidus and the eutectic transition. To increase the sensitivity for high cooling rates Figure 6 f) shows the change of the cooling rate dT/dt as a function of time. In Figure 6 d) and e) the release of latent heat during solidification leads to a positive deviation

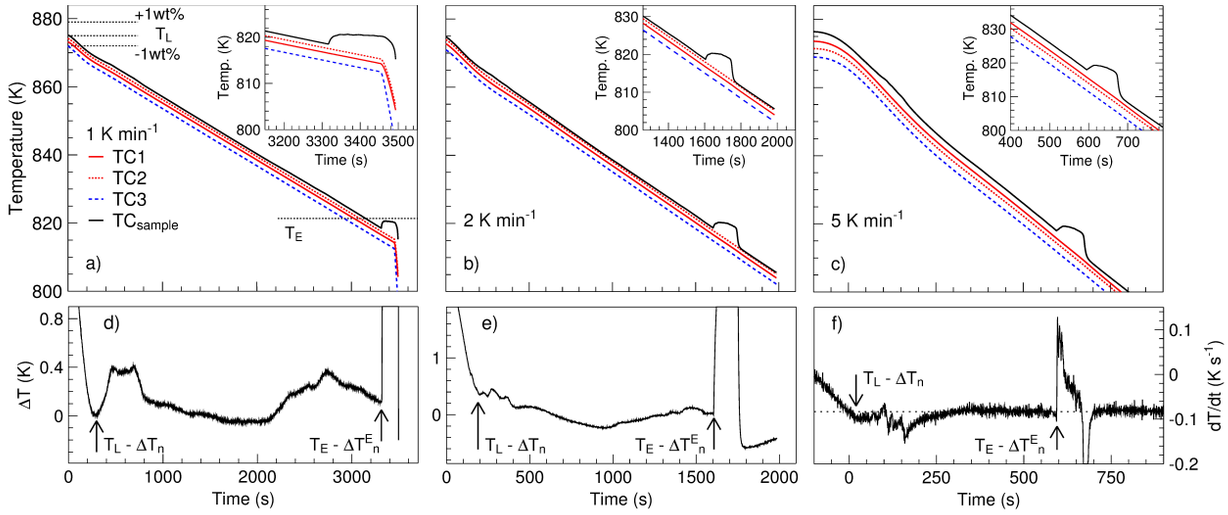

6.jpg

FIG. 6. Temperature vs. time plot of an Al-20wt.%Cu sample inoculated with 0.01 wt.% Al-5Ti-1B. The thermocouples (TC1-TC3) measure the temperature at different positions inside the furnace. TC_{Sample} is located inside the melt. For comparison three different cooling rates (1 K min^{-1}, 2 K min^{-1} and 5 K min^{-1}) were applied successively to the same sample (a-c). (d) and (e) show the temperature deviation from an ideal constant cooling curve and (f) shows the change in cooling rate with time. The liquidus temperature T_L and the eutectic temperature T_E of the alloy are displayed in the plot (e-f). In case of the event of the formation of a first crystal in the melt (T_L-T_n) and when the eutectic phase transition occurs (T_E- $T^E{}_n$) spontaneous heat release in the TC_{Sample} cooling curves can be monitored. Reprinted with permission from M.Wegener, Morphological transitions in Al-Ge alloys observed with in-situ X-radiography, Ph.D. dissertation (RWTH Aachen University, 2021[25]).

of the temperature. This is particularly pronounced for the eutectic transition. In Figure 6 f) a solidification event leads to a change of the cooling rate which is initially positive and, later during the transformation, more negative than the applied cooling rate. In all cases nucleation undercooling can be observed. The temperature arrest, attributed to the eutectic reaction is clearly visible (cf. inset Figure 6 a-c). It shows a small plateau in temperature. The plateau is more persistent for low cooling rates as they are closer to equilibrium conditions. The equilibrium phase diagram reports an eutectic temperature of 821.4 K[28]. The plateau temperature for 1 K min^{-1} cooling rate is 820.6 K for 2 K min^{-1} it is 820.3 K and for 5 K min^{-1} it is 819.3 K. Extrapolating the data to an ideal zero cooling rate obtains an eutectic temperature of 820.9 K which is within 0.5 K to the phase diagram value. To further validate temperature homogeneity within the sample, images during solidification were analyzed. Since a thermocouple, place inside the melt, acts as a heat sink and triggers the nucleation of dendrites next to it, only for calibrating the furnace TC_{Sample} was placed inside the melt. The results are presented in Figure 6. All other experiments were performed without a thermocouple in direct contact with the melt. Figure 7 shows a solidification sequence for the Al-20 wt.%Ge processed in ITF2. First, a cooling rate of 10 K min^{-1} was applied to ensure high nucleation undercooling and activate the grain refiner particles. The grains start to nucleate at 889.3 K, homogenously distributed in the melt and grow dendritically (Figure 7 a-c). When the grains start to impinge, the sample temperature was increased again up to 888.1 K until the grains were almost no longer visible in the FOV (cf. Figure 7 d)) as the dendritic branches were dissolved and only solid cores remained. From this stage, a low cooling rate of 0.1 K min^{-1} was applied. The process is comparable to semi-solid processing techniques like rheo- or thixo-casting where solid particles are added to the melt before solidification[29]. The grains grow slowly with globulitic shapes. Figure 7 e) and f) show that the Aluminum dendrites coarsen continuously over time without the observation of temperature gradient zone melting towards the rim. This indicates an extremely small or absent temperature gradient in the sample. Another indication of homogeneous heat input is the nucleation of dendrites equally distributed in the melt. Beside the homogeneity of the distribution on growth of the dendrites in the melt, at this point it should be noted, that neither the placement of the heaters in the X-ray beam path, nor the additional insulation material in the path are affecting the quality of the X-ray images. An additional solidification sequence of an Al-20 wt.%Cu sample inoculated with 0.01 wt.%Al-5Ti-1B is shown in Figure 8. The sample is horizontally aligned and cooled down at a rate of 15 K min^{-1}. The addition of Titanium-Boron-based particles controls the necessary nucleation undercooling to activate particles of a certain size depending on a given cooling rate[22]. As a consequence, all dendrites start to nucleate at the same temperature if no thermal gradient is present in the melt. Due to the spatial resolution of 3 the exact start point of the nucleation process is not detectable. However, it can be expected that grains nucleating with a certain separation are subjected to similar growth conditions and hence, after a certain period of time, reach a similar detectable size. In Figure 8 a) small, equally distributed grains can be observed. This indicates an isothermal temperature field in the melt. With continuing solidification, the dendrites grow larger until the

eutectic temperature is reached. When the eutectic temperature is reached, the eutectic front is propagating through the FOV. This point is well-defined, since T_E has a precisely-defined temperature and is known from the phase diagram[28]. The front is clearly visible as it contrasts from the melt in dark grey due to a density change between liquid melt and eutectic solid. The evolution of the eutectic transformation in the melt is displayed in Figure 8 b)-f). For better visibility of the propagating eutectic front, the Aluminum dendrites have been subtracted in the Figure 8 b)-f) using image processing techniques. The eutectic front starts in the center of the sample, as well as in the upper right corner and grows radially, with a square morphology. It is not assumed that the square morphology comes from an influence of thermocouples TC1-TC3, since the "edges" of the square do not point directly to the thermocouples and, moreover, there are only three thermocouples arranged around the sample. It is more likely, that the morphology is a growth phenomenon, reflecting growth orientation relationships between the Al-Al_2Cu eutectic, as it was for example reported by Davies and Hellawell[30] or Li et al.[31] for regular eutectic growth. Whether the square morphology is indeed a growth phenomenon needs further investigation, e.g., by electron microscopy of the eutectic phase. In total, the nucleation front needs approximately 20 seconds to propagate through the FOV. Different melting cycles of this sample and of other Al-Ge sample systems show similar results. However, the starting point of the eutectic front is typically randomly located in the FOV and in most cases a second (upper right corner of Figure 8 c)-f)) or even third starting point can be observed. This is a third indicator for a homogeneous temperature distribution in the melt.

7.jpg

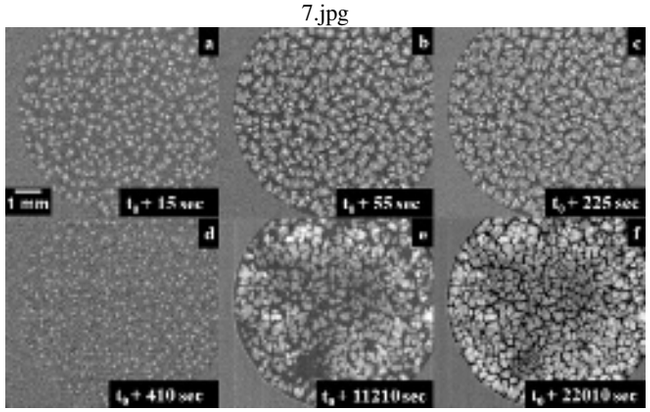

FIG. 7. Solidification cycle for an Al-20 wt.% Ge sample, inoculated with 1 wt.%Al-5Ti-1B. In a first step; cooling rates of $10\,\mathrm{K\,min^{-1}}$ were applied to trigger grain nucleation and grain growth (a-c). Then, the dendrites were re-melted to small nucleation spots and afterwards solidified with $0.1\,\mathrm{K\,min^{-1}}$(d). Globulitic-like morphologies develop from the small re-melted grain nucleation spots. Observation over time shows a steady coarsening. Two different long-term solidification steps are featured in picture e) and f). Reprinted with permission from M.Wegener, Morphological transitions in Al-Ge alloys observed with in-situ X-radiography, Ph.D. dissertation (RWTH Aachen University, 2021[25]).

8.jpg

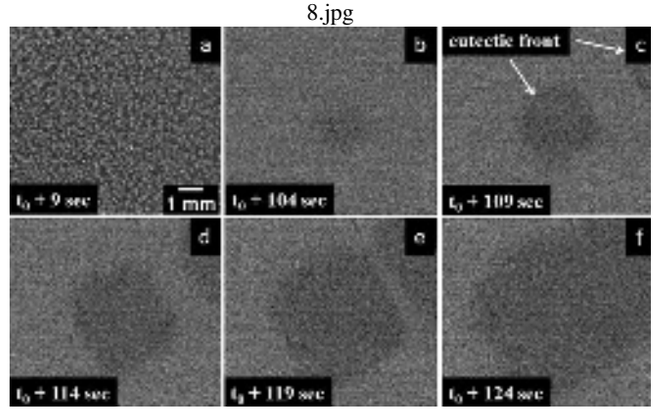

FIG. 8. Al-20 wt.% Cu + 0.01 wt.%Al-5Ti-1B sample solidified with $15\,\mathrm{K\,min^{-1}}$. The first image (a) of radiographs displays the nucleation of Aluminum-dendrites in the isothermal melt. t_0 corresponds to the first appearance of dendrites in the sample. The Aluminum dendrites have been removed from the images b)-f) for better visibility of the eutectic front. After 104 seconds, the temperature reaches the eutectic temperature and the melt transforms, which can be detected as dark grey front moving through the FOV. Images b)-f) show the propagation of the eutectic front through the FOV. Reprinted with permission from M.Wegener, Morphological transitions in Al-Ge alloys observed with in-situ X-radiography, Ph.D. dissertation (RWTH Aachen University, 2021[25]).

V. CONCLUSION AND OUTLOOK

In our previous furnace design[7] heat input coming from the direction of the sample borders resulted in a cooling-rate dependent radial temperature gradient of e. g. $0.1\,\mathrm{K\,mm^{-1}}$ at $1\,\mathrm{K\,min^{-1}}$ cooling rate with a cooler sample center. This small gradient lead to several effects, causing remelting of the dendrites in the outer zone of the sample and coarsening in the sample center. A new X-ray transparent isothermal furnace setup was designed and characterized with the aim to generate a homogeneous temperature field inside the melt avoiding TGZM in long-term experiments. The introduction of a X-ray transparent heating foil above and below the sample led to a major improvement in homogeneity. The temperature field was directly characterized by thermocouples embedded not only in the furnace but also in the sample. Solidification experiments on inoculated samples demonstrated the homogeneity of the temperature field in the sample. It has been shown that the furnace can be used to undertake semi-solid processing and long-term grain coarsening experiments in combination with in-situ X-radiography. Hence, this furnace enables the investigation of the transition from globulitic growth of nuclei in the early stages of solidification to dendritic growth at a later stage. It also allows investigation of the evolution of the form and size of coarsened dendrites and their solute fields.

ACKNOWLEDGMENTS

We thank the workshop team of the Institute M. Nell, K. Afanasev, H. Esser and R. Henrichs for the support getting the furnace parts ready, D. Bräuer for the fruitful discussions on temperature measurement techniques and heater control system and J. Drescher for his input and support during the furnace development.

VI. DATA AVAILABILITY

The data that support the findings of this study are available from the corresponding author upon reasonable request.

[1]R. H. Mathiesen, L. Arnberg, F. Mo, T. Weitkamp, and A. Snigirev, "Time resolved x-ray imaging of dendritic growth in binary alloys," Physical Review Letters **83**, 5062–5065 (1999).

[2]A. G. Murphy, D. J. Browne, W. U. Mirihanage, and R. H. Mathiesen, "Combined in situ x-ray radiographic observations and post-solidification metallographic characterisation of eutectic transformations in al–cu alloy systems," Acta Materialia **61**, 4559–4571 (2013).

[3]H. Nguyen Thi, G. Reinhart, A. Buffet, T. Schenk, N. Mangelinck-Noël, H. Jung, N. Bergeon, B. Billia, J. Härtwig, and J. Baruchel, "In situ and real-time analysis of tgzm phenomena by synchrotron x-ray radiography," Journal of Crystal Growth **310**, 2906–2914 (2008).

[4]M. P. Stephenson and J. Beech, "In–situ observations of solute redistribution during solidification," Solidification and Casting of Metals **425**, 34–39 (1977).

[5]W. Kaukler and F. Rosenberger, "X–ray microscopic observations of metal solidification dynamics," Metallurgical and Materials Transactions A **25A**, 1775–1777 (1994).

[6]C. Rakete, C. Baumbach, A. Goldschmidt, D. Samberg, C. G. Schroer, F. Breede, C. Stenzel, G. Zimmermann, c. Pickmann, Y. Houltz, C. Lockowandt, O. Svenonius, P. Wiklund, and R. H. Mathiesen, "Compact x–ray microradiograph for in situ imaging of solidification processes: Bringing in situ x–ray micro-imaging from the synchrotron to the laboratory," Review of Scientific Instruments **83**, 1–10 (2011).

[7]M. Becker, C. Dreißigacker, S. Klein, and F. Kargl, "Near-isothermal furnace for in situ and real time x-ray radiography solidification experiments," The Review of scientific instruments **86**, 063904 (2015).

[8]A. G. Murphy, R. H. Mathiesen, Y. Houltz, J. Li, C. Lockowandt, K. Henriksson, G. Zimmermann, N. Melville, and D. J. Browne, "Xrmon-sol: Isothermal equiaxed solidification of a grain refined al–20wt%cu alloy," Journal of Crystal Growth **440**, 38–46 (2016).

[9]H. Nguyen-Thi, G. Reinhart, G. Salloum Abou Jaoude, R. H. Mathiesen, G. Zimmermann, Y. Houltz, D. Voss, A. Verga, D. J. Browne, and A. G. Murphy, "Xrmon–gf: A novel facility for solidification of metallic alloys with in situ and time-resolved x-ray radiographic characterization in microgravity conditions," Journal of Crystal Growth **374**, 23–30 (2013).

[10]M. Becker, S. Klein, and F. Kargl, "Free dendritic tip growth velocities measured in al–ge," Physical Review Materials **2** (2018), 10.1103/PhysRevMaterials.2.073405.

[11]A. G. Murphy, R. H. Mathiesen, Y. Houltz, J. Li, C. Lockowandt, K. Henriksson, N. Melville, and D. J. Browne, "Direct observation of spatially isothermal equiaxed solidification of an al–cu alloy in microgravity on board the maser 13 sounding rocket," Journal of Crystal Growth **454**, 96–104 (2016).

[12]G. Salloum-Abou-Jaoude, H. Nguyen-Thi, G. Reinhart, R. H. Mathiesen, G. Zimmermann, and D. Voss, "Characterization of motion of dendrite fragment by x-ray radiography on earth and under microgravity environment," Materials Science Forum **790-791**, 311–316 (2014).

[13]F. Kargl, J. Drescher, C. Dreißigacker, M. Balter, M. Becker, M. Wegener, and E. Sondermann, "Xrise-m: X-radiography facility for solidification and diffusion studies of alloys aboard sounding rockets," The Review of scientific instruments **91**, 013906 (2020).

[14]A. Bogno, H. Nguyen-Thi, G. Reinhart, B. Billia, and J. Baruchel, "Growth and interaction of dendritic equiaxed grains: In situ characterization by synchrotron x-ray radiography," Acta Materialia **61**, 1303–1315 (2013).

[15]Y. Z. Li, N. Mangelinck-Noël, G. Zimmermann, L. Sturz, and H. Nguyen-Thi, "Comparative study of directional solidification of al-7 wt% si alloys in space and on earth: Effects of gravity on dendrite growth and columnar-to-equiaxed transition," Journal of Crystal Growth **513**, 20–29 (2019).

[16]L. Abou-Khalil, G. Salloum-Abou-Jaoude, G. Reinhart, C. Pickmann, G. Zimmermann, and H. Nguyen-Thi, "Influence of gravity level on columnar-to-equiaxed transition during directional solidification of al–20 wt.% cu alloys," Acta Materialia **110**, 44–52 (2016).

[17]H. Nguyen-Thi, G. Reinhart, and B. Billia, "On the interest of microgravity experimentation for studying convective effects during the directional solidification of metal alloys," Comptes Rendus Mécanique **345**, 66–77 (2017).

[18]S. Zabler, A. Rueda, A. Rack, H. Riesemeier, P. Zasansky, I. Manke, F. Garcia-Moreno, and J. Banhart, "Coarsening of grain-refined semi-solid al–ge32 alloy: X-ray microtomography and in situ radiography," Acta Materialia **55**, 5045–5055 (2007).

[19]H. Neumann-Heyme, N. Shevchenko, Z. Lei, K. Eckert, O. Keplinger, J. Grenzer, C. Beckermann, and S. Eckert, "Coarsening evolution of dendritic sidearms: From synchrotron experiments to quantitative modeling," Acta Materialia **146**, 176–186 (2018).

[20]R. H. Mathiesen, L. Arnberg, P. Bleuet, and A. Somogyi, "Crystal fragmentation and columnar-to-equiaxed transitions in al-cu studied by synchrotron x-ray video microscopy," Metallurgical and Materials Transactions A **37**, 2515–2524 (2006).

[21]E. Liotti, A. Lui, S. Kumar, Z. Guo, C. Bi, T. Connolley, and P. S. Grant, "The spatial and temporal distribution of dendrite fragmentation in solidifying al-cu alloys under different conditions," Acta Materialia **121**, 384–395 (2016).

[22]A. L. Greer, "Overview: Application of heterogeneous nucleation in grain-refining of metals," The Journal of chemical physics **145**, 211704 (2016).

[23]G. Reinhart, H. Nguyen-Thi, B. Sarpi, A. Bogno, and B. Billia, "In situ investigation of grain migration by tgzm during solidification in a temperature gradient," Materials Science Forum **790-791**, 323–328 (2014).

[24]S. Klein, D. Bräuer, M. Becker, A. Knipstein, S. Meckel, E. Sondermann, and F. Kargl, "X-rise - a multifunctional x-ray radiography device for parabolic flights and laboratory use," International Journal of Microgravity Science and Application **33**, 330405 (2016).

[25]M. Wegener, "Morphological transitions in al-ge alloys observed with in-situ x-radiography," Publikationsserver, RWTH Aachen University 2021 , 1–152 (2019, 2021).

[26]M. Becker, J. A. Dantzig, M. Kolbe, S. T. Wiese, and F. Kargl, "Dendrite orientation transition in al–ge alloys," Acta Materialia **165**, 666–677 (2019).

[27]F. Islam, A. K. Thykadavil, and M. Medraj, "A computational thermodynamic model of the mg–al–ge system," Journal of Alloys and Compounds **425**, 129–139 (2006).

[28]W. D. Callister, *Materials science and engineering: An introduction*, 7th ed. (Wiley, New York, NY, 2007).

[29]A. Pola, M. Tocci, and P. Kapranos, "Microstructure and properties of semi-solid aluminum alloys: A literature review," Metals **8**, 181 (2018).

[30]I. G. Davies and A. Hellawell, "Phase orientations in the lamellar and non-lamellar regions of the al-cual2 eutectic alloy," The Philosophical Magazine: A Journal of Theoretical Experimental and Applied Physics **22**, 1255–1259 (1970).

[31]X. Li, J. Wang, L. Hou, A. Gagnoud, and Y. Fautrelle, "Studying on the morphology of primary phase by 3d-ct technology and controlling eutectic growth by tailoring the primary phase," Journal of Alloys and Compounds **821**, 153457 (2020).

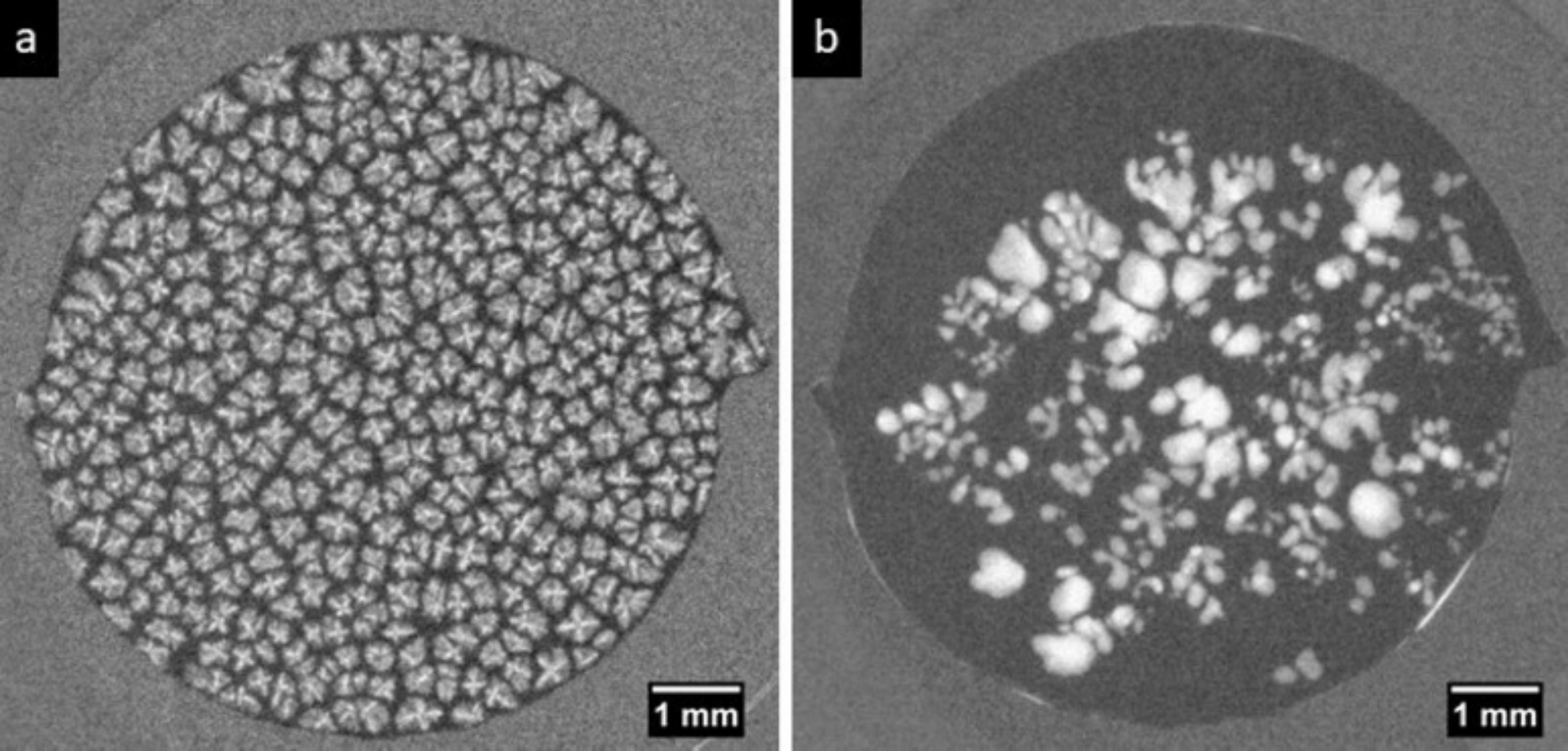
a
1 mm
b
1 mm

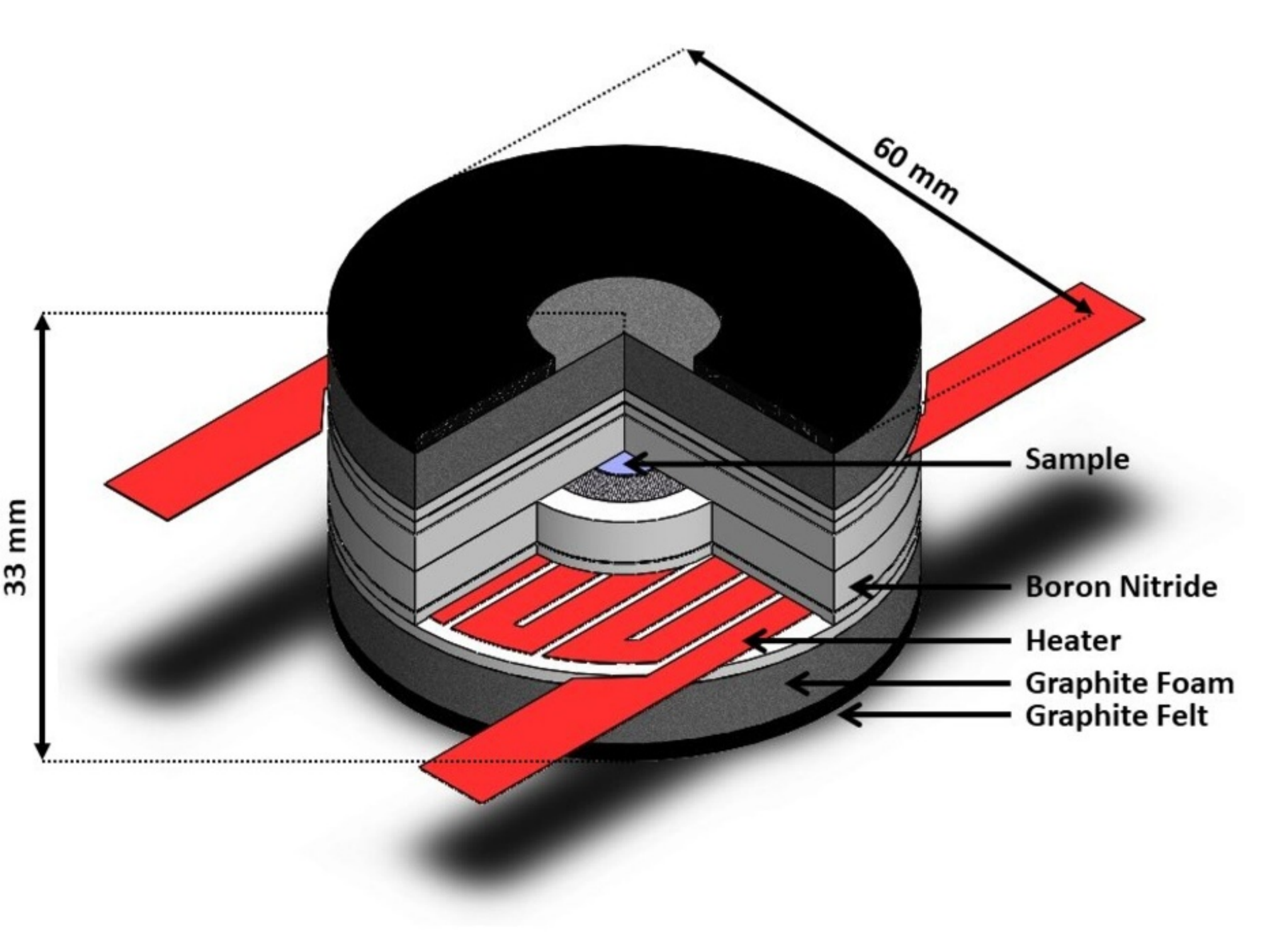
60 mm
33 mm
Sample
Boron Nitride
Heater
Graphite Foam
Graphite Felt

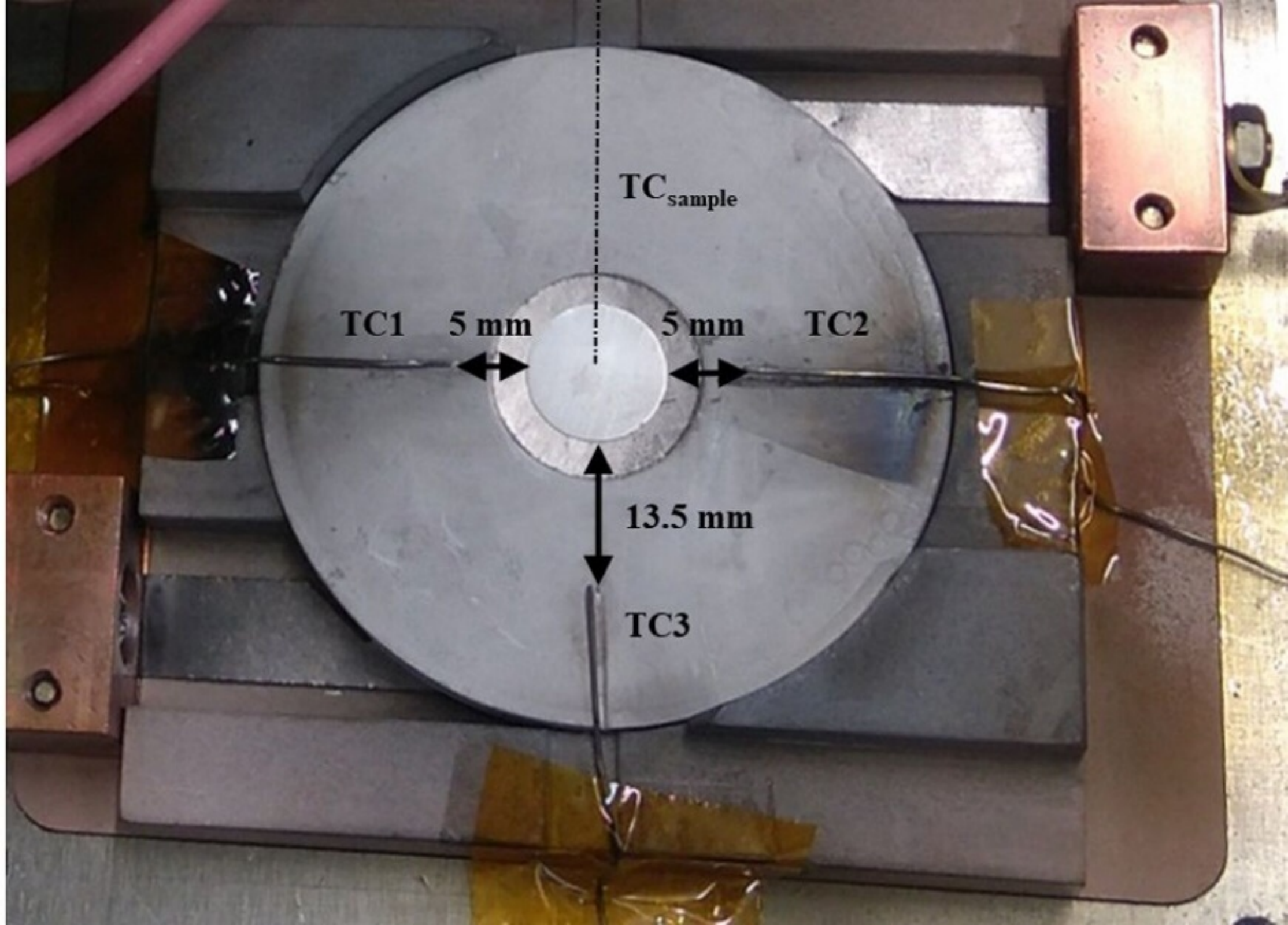
TC$_{sample}$
TC1
5 mm
5 mm
TC2
13.5 mm
TC3

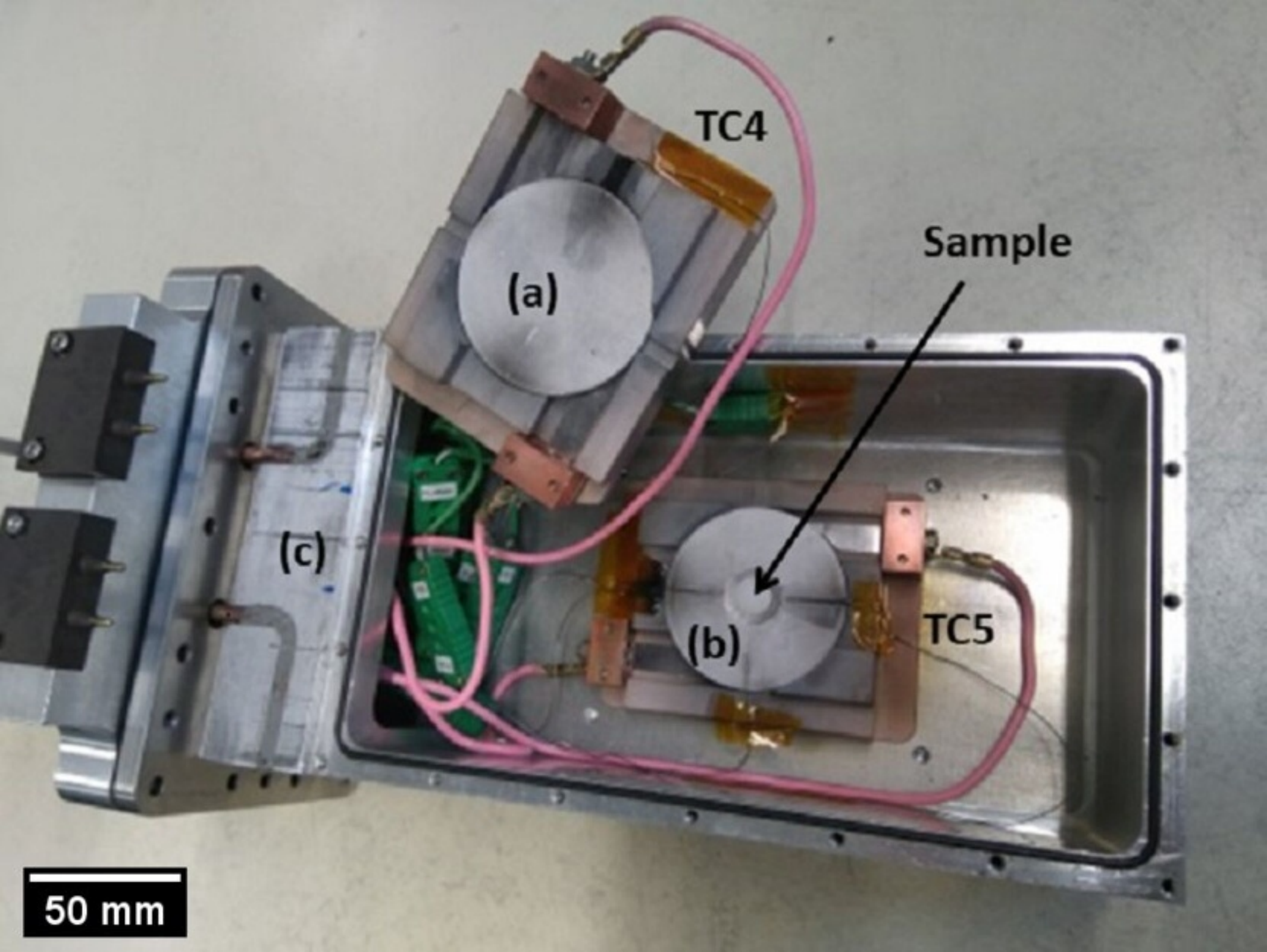
TC4
Sample
(a)
(c)
(b)
TC5
50 mm

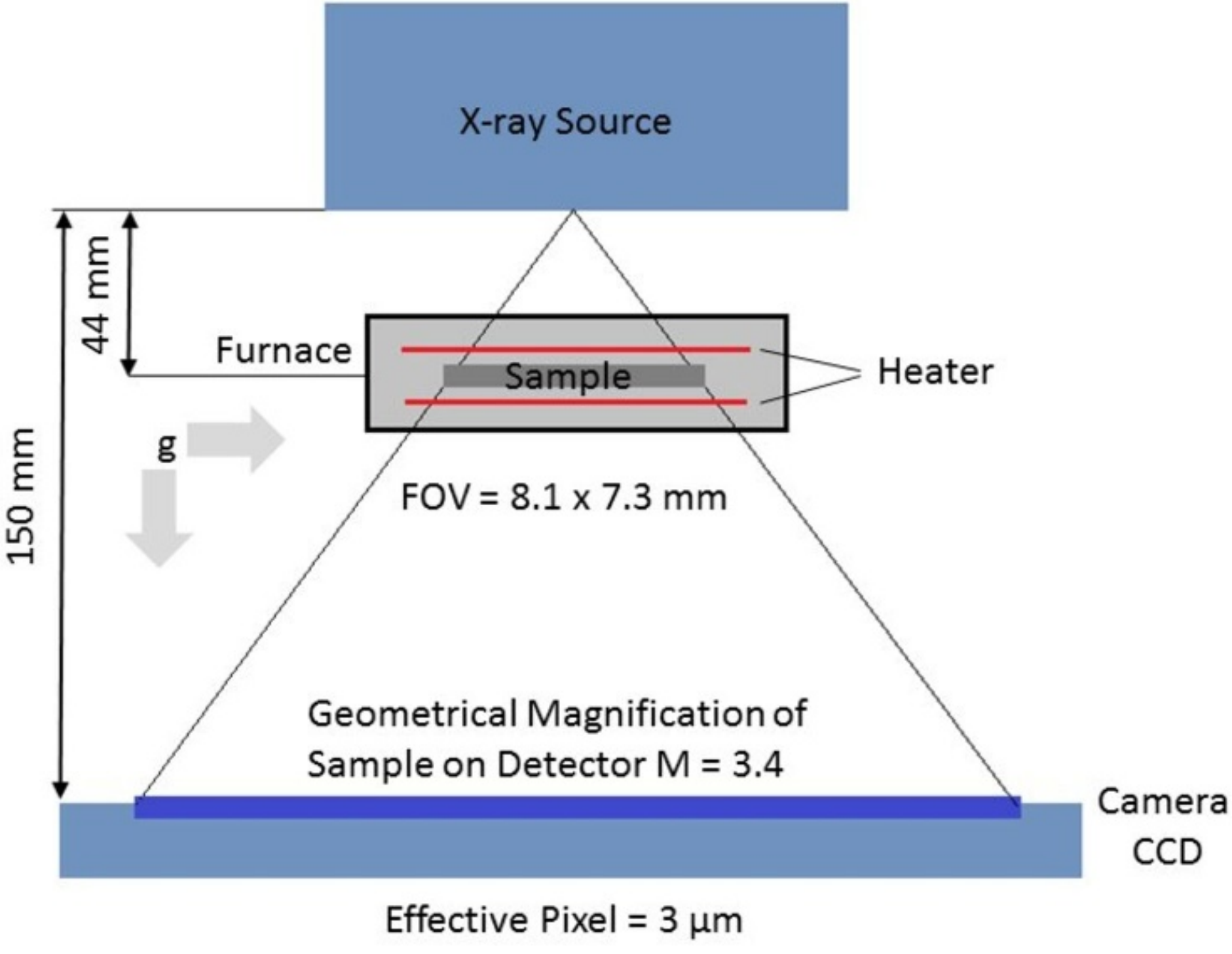
X-ray Source
44 mm
Furnace
Sample
Heater
g
150 mm
FOV = 8.1 x 7.3 mm
Geometrical Magnification of
Sample on Detector M = 3.4
Camera
CCD
Effective Pixel = 3 µm

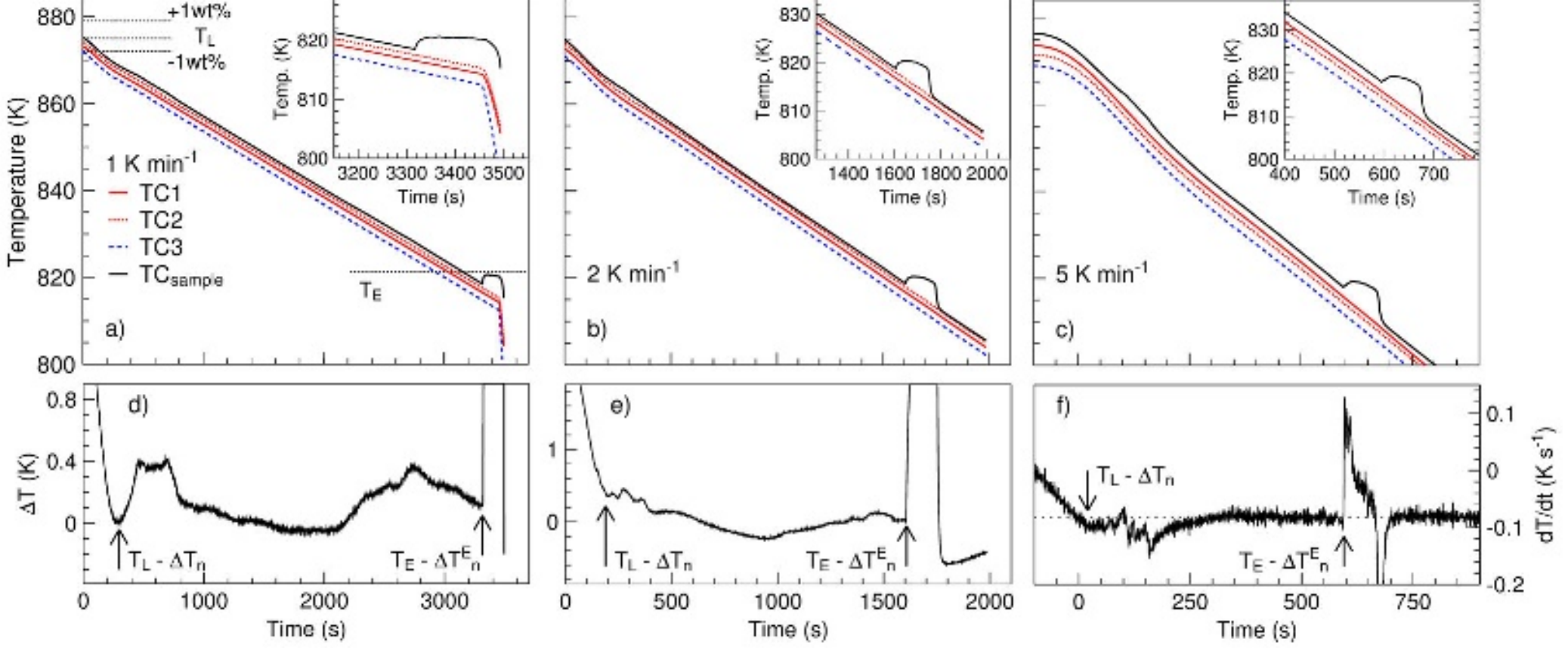
Temperature (K)
+1wt%
T_L
-1wt%
1 K min^{-1}
TC1
TC2
TC3
TC_{sample}
T_E
a)
Temp. (K)
Time (s)
2 K min^{-1}
b)
5 K min^{-1}
c)
ΔT (K)
d)
e)
f)
T_L - ΔT_n
T_E - ΔT^E_n
dT/dt (K s^{-1})

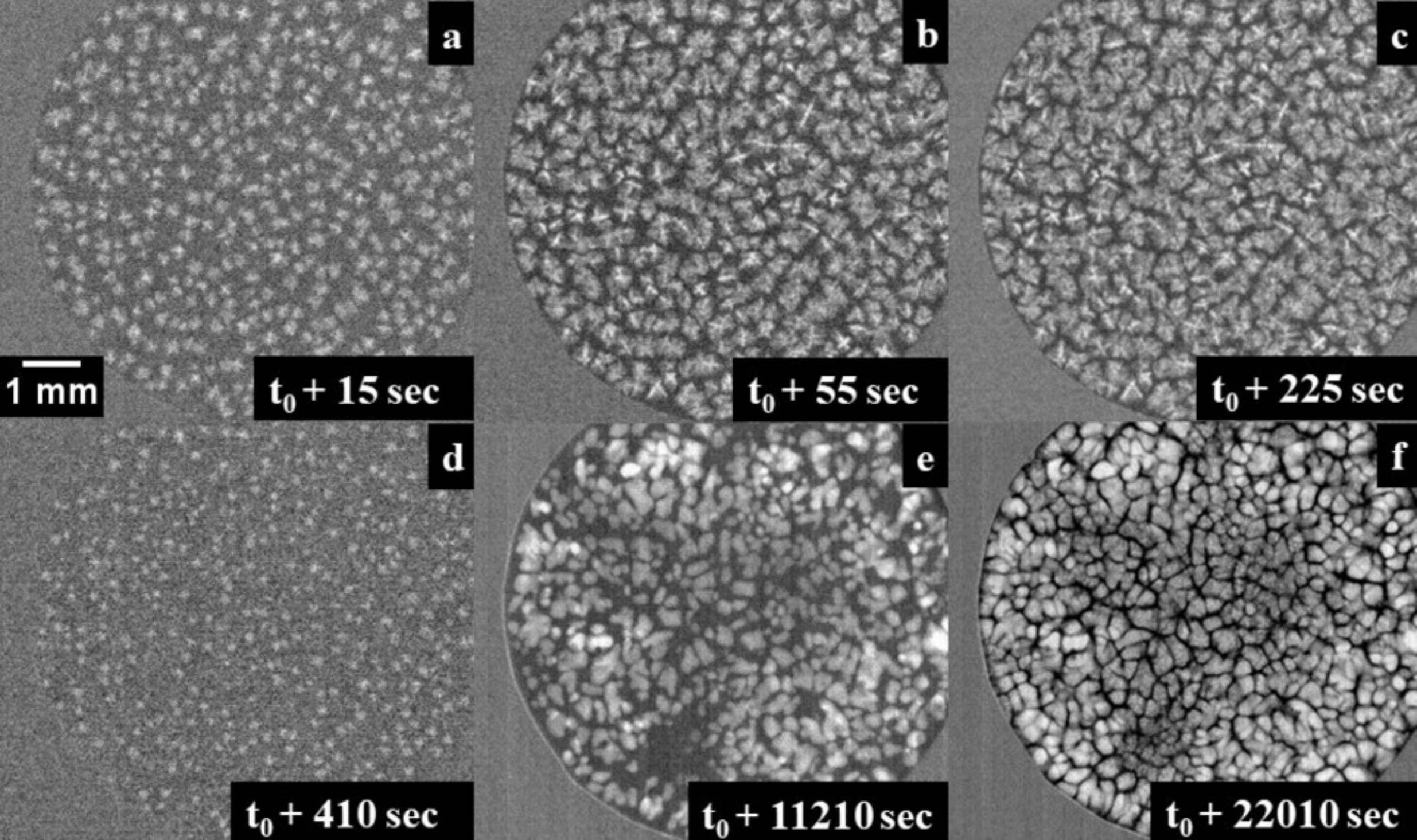
a
b
c
1 mm
t_0 + 15 sec
t_0 + 55 sec
t_0 + 225 sec
d
e
f
t_0 + 410 sec
t_0 + 11210 sec
t_0 + 22010 sec

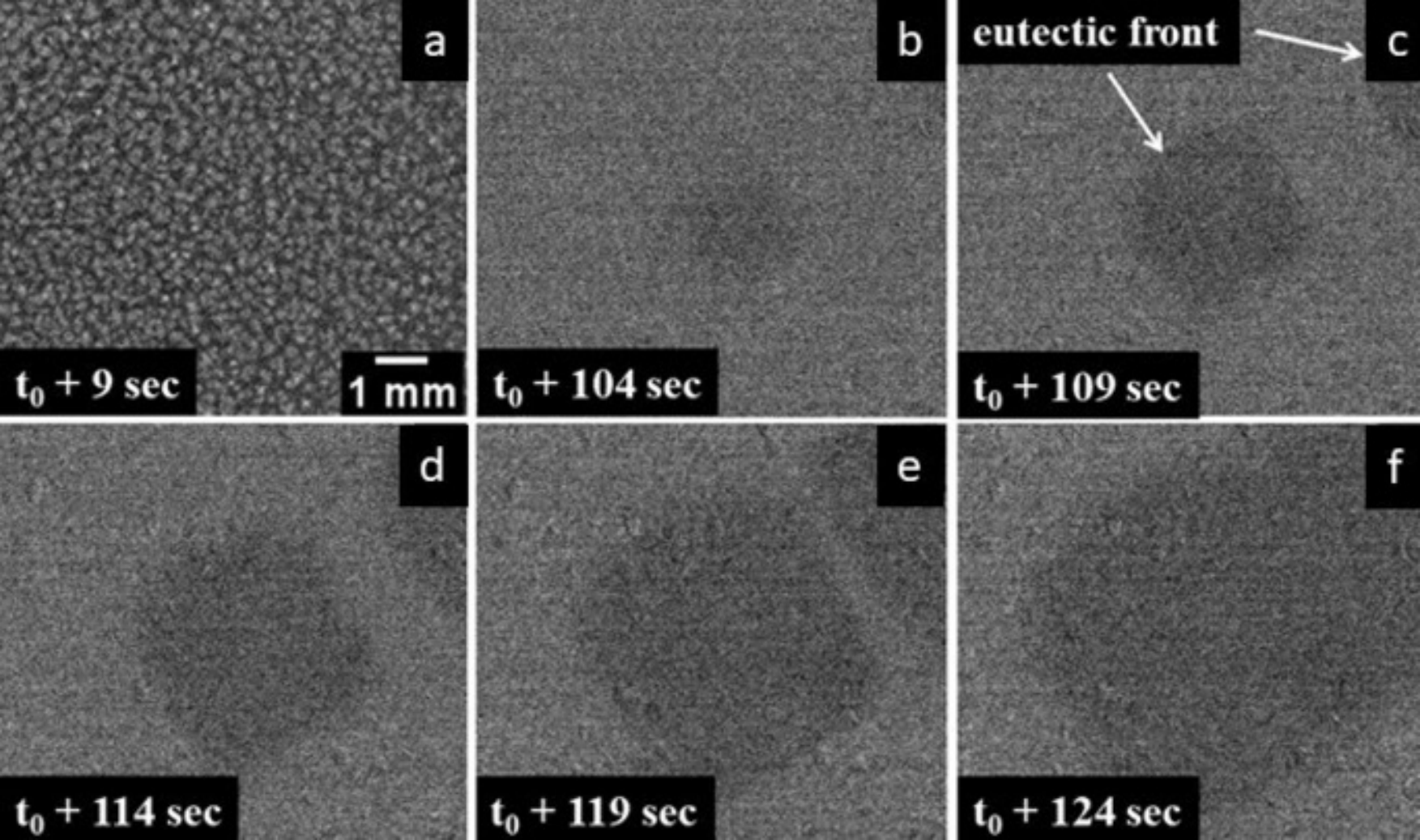
a
b
eutectic front
c
t_0 + 9 sec
1 mm
t_0 + 104 sec
t_0 + 109 sec
d
e
f
t_0 + 114 sec
t_0 + 119 sec
t_0 + 124 sec